


RESEARCH

Open Access



Numerical methods to simulate moisture dynamics in fibrous sheet

Hidekazu Yoshioka* , Kotaro Fukada and Ichiro Kita

*Correspondence:
yoshih@life.shimane-u.ac.jp
Faculty of Life and Environmental
Science, Shimane University,
Nishikawatsu-cho 1060, Matsue,
Shimane, 690-8504, Japan

Abstract

Comprehension of moisture dynamics in fibrous sheets is indispensable in a wide variety of industrial areas. This paper proposes a practical mathematical model, which is referred to as the 2-D extended porous medium equation (PME), to physically describe moisture dynamics in fibrous sheets under evaporative environment. A numerical method, which is referred to as the 2-D dual-finite volume method (DFVM), to approximate its solutions in a stable manner is also presented so that the moisture dynamics is reasonably simulated. The 2-D DFVM, which can optionally be equipped with isotone numerical fluxes, is examined with test cases to show its satisfactory accuracy and versatility. The parameters and coefficients involved in the mathematical model for a non-woven fibrous sheet are identified with laboratory experiments. Numerical simulation of moisture dynamics in the horizontally or vertically placed sheet is performed as a demonstrative application example of the present model and the numerical method.

Keywords: fibrous sheets; moisture dynamics; extended porous medium equations; dual finite volume method; non-woven fibrous sheets

1 Introduction

Comprehension of moisture dynamics in fibrous sheets are necessary in a wide variety of industrial areas, such as chemical engineering [1, 2], environmental engineering [3, 4], precise agriculture [5], and sanitary engineering [6]. Moisture dynamics in porous media such as fibrous sheets is macroscopic appearance of microscopic liquid water transport in multiply-connected pore network structures [7, 8]. In practical applications, moisture dynamics both in fibrous sheets and on their surface, the latter is due to evaporation driven by the humidity dynamics between the sheets and atmosphere [9, 10], is of importance for manufacturing better products in paper and textile industry [11–13]. Assessing moisture dynamics in non-woven fibrous sheets is therefore indispensable for development of products that are better fit-for-purpose.

Moisture dynamics occurring in the fibrous sheets have been described with nonlinear conservation laws based on the classical fluid dynamics [14, 15]. Numerically approximating solutions to nonlinear conservation laws requires applications of a conservative and stable numerical method, so that reasonable numerical solutions are obtained, such that positivity and/or monotonicity of certain physical quantities are realized. One common numerical method for nonlinear conservation laws is the finite volume method (FVM)

based on local conservation principles [16]. The core of the FVM is evaluating numerical fluxes on cell interfaces, which determine accuracy and stability of numerical solutions [17, 18]. For solving conservation laws with dominant advection in particular, numerical fluxes should guarantee unconditional stability in space and should possess least numerical diffusion effects. This issue is more delicate for degenerate conservation laws than for those with non-degenerate counterparts because of possibly vanishing diffusion coefficients [19–21]. Mathematically, degeneration of the diffusion coefficients significantly affects qualitative behavior of the solutions to the conservation laws [22, 23]. Degeneration of diffusion coefficients would cause numerical instabilities even with sufficiently fine meshes when a standard numerical method is utilized [24]. Handling source terms in nonlinear partial differential equations like conservation laws also requires devised techniques for stable computation [25, 26]. Analyzing the moisture dynamics that we focus on would require sophisticated numerical techniques due to its complexity, which is our motivation of writing this paper with a particular emphasis on numerics.

This paper focuses on an FVM for porous medium equations (PMEs), which govern moisture dynamics in porous media, such as soils [27–29], fibrous sheets [4, 30, 31], and debris materials [32]. Similar differential equations are encountered in different physical problems, such as heat conduction problems in plasma [33, 34], combustion of liquids [35, 36], evaporation dynamics of volatile liquids [37], chemotaxis of cells and organisms [38, 39], and astrophysics [40]. Detailed, extensive mathematical and numerical analyses on the PME have been performed so far [41–43]. Zambra et al. [44] proposed an oscillation-free FVM with the weighted essentially non-oscillatory interpolation. The Discontinuous Galerkin methods are finite volume analogues of finite element methods, which also are conservative [44, 45]. Finite Volume Element Methods are conservative methods that concurrently use finite element and finite volume discretization schemes, which have also been effectively used for PMEs [46, 47].

Literature indicate that the concept of the isotonicity on numerical fluxes, originally stated in Ortega and Rheinboldt [48] and has later been discussed in Fuhrmann and Langmach [49], can possibly help develop stable and physically consistent FVMs in a simple manner. According to Fuhrmann and Langmach [49], numerical fluxes in the FVMs for nonlinear conservation laws such as PMEs should equip with the isotonicity for computing oscillation-free numerical solutions without extremely fine computational meshes. Their numerical fluxes for the conventional PMEs are isotone and can compute oscillation-free and non-negative numerical solutions; however, they would not be suitable for the PMEs of moisture dynamics in fibrous sheets as later demonstrated in this paper.

The purpose of this paper is to propose and examine a practical, stable FVM for 2-D PME-type equations that is referred to as the 2-D dual-finite volume method (DFVM), focusing in particular on application to moisture dynamics in fibrous sheets under evaporative environment. The governing equation of the moisture dynamics is an extended PME having nonlinear advection and evaporation terms [6, 50]. Yoshioka and Unami [51] originally proposed a prototype DFVM for simulating solute dispersion phenomena in surface water networks (connected graphs) consisting of 1-D reaches (lines or curves) and 0-D junctions (vertices). Yoshioka et al. [6] and Yoshioka and Triadis [50] later extended the DFVM for nonlinear conservation laws in 1-D domains and connected graphs. The original DFVM is unconditionally stable in space for linear parabolic equations and is unconditionally stable in both space and time when equipped with a fully-implicit temporal

discretization method [51]. Numerical fluxes are evaluated with analytical solutions to linearized local two-point boundary value problems in the DFVM. This numerical technique is referred to as the fitting technique. Fitting technique have successfully been used for solving differential equations encountered in a variety of problems, such as option pricing [52, 53], optimal controls [54], and reactive transport phenomena [55, 56]. Numerical fluxes with the fitting technique guarantee first-order spatial convergence for linear problems [57, 58]. This paper provides an isotone numerical flux specialized for the 2-D extended PME and its application to test cases and a realistic problem. Stability of the present DFVM for the extended PME is achieved with a new isotone numerical flux. Nonlinear source terms involved in the extended PME are dealt with using an operator-splitting technique [59] to compute stable and physically consistent numerical solutions.

The rest of this paper is organized as follows. Section 2 presents the 1-D and 2-D PMEs. Their regularized counterparts for well-posing the problems are also presented in this section, which are used in numerical computation in this paper. Section 3 presents the discretization procedure of the 2-D DFVM. Section 4 presents applications of the 2-D DFVM and 2-D extended PME to test cases and a realistic problem. Section 5 concludes this paper.

2 Mathematical model

The extended PMEs for moisture dynamics in fibrous sheets subject to evaporation are presented. The 1-D extended PME [50], although it is not explicitly used in this paper, is firstly presented as a reduced counterpart of the present 2-D model for self-contentedness.

2.1 1-D extended porous medium equation

The 1-D extended PME was formulated for simulating 1-D longitudinal moisture dynamics occurring in porous media with a striped shape. It is physically reasonable to assume that moisture profiles in such a sheet are transversely homogenous, leading to a longitudinally 1-D model. The saturation at each longitudinally 1-D position x of a sheet at the time t is denoted by $\theta = \theta(t, x)$, and is normalized in $[0, 1]$ as $0 \leq u = (\theta - \theta_r)(\theta_s - \theta_r)^{-1} \leq 1$ where θ_s and θ_r are the maximum (saturated) and minimum (residual) water contents of the sheet.

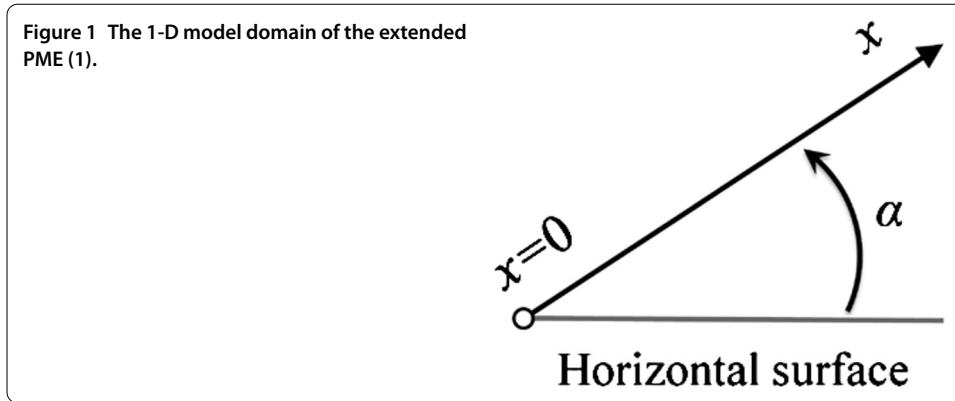
Based on the non-dimensionalization method [60], the 1-D extended PME is presented as [4, 31]

$$\frac{\partial u}{\partial \tilde{t}} = \frac{\partial}{\partial \tilde{x}} \left((m-p)u^{m-p-1} \frac{\partial u}{\partial \tilde{x}} \right) + \sin \alpha \frac{\partial}{\partial \tilde{x}} (u^{m-1}u) - \tilde{E}_s u^q \tag{1}$$

subject to appropriate initial and boundary conditions with the non-dimensional variables

$$\tilde{t} = \frac{K_s^2(m-p)}{D_s \theta_s^2} t, \quad \tilde{x} = \frac{K_s(m-p)}{D_s \theta_s} x, \quad \text{and} \quad \tilde{E}_s = \frac{D_s \theta_s^2}{K_s^2(m-p)} E_s, \tag{2}$$

where $D_s (> 0)$ is the saturated diffusivity, $K_s (> 0)$ is the saturated permeability, $E_s (\geq 0)$ is the evaporation coefficient, $m, p \leq m - 1$, and $0 < q < 1$ are positive nonlinearity parameters determining nonlinearity of (1), and $-0.5\pi \leq \alpha \leq 0.5\pi$ is the inclination angle of the sheet as depicted in Figure 1. A remarkable difference between the extended PME (1) and the conventional models for moisture dynamics in fibrous sheets [31, 61] is that the former can simulate the evaporative moisture dynamics that the latter in principle cannot do



because of the absence of a source term to describe the effect of evaporation. According to the standard theory of evaporation from porous media, it is only as the saturation $u \ll 1$ that the evaporation rate rapidly decreases to zero [62]. The pressure head $\psi(u)$ and the hydraulic permeability $K(u)$ consistent with the 1-D extended PME (1) are

$$\psi(u) = \frac{\theta_s D_s}{p K_s} \left(1 - \frac{1}{u^p} \right) \quad \text{and} \quad K(u) = K_s u^m, \tag{3}$$

respectively. The former reduces to the conventional model when $p \rightarrow +0$ [4, 31]:

$$\psi(u) = \frac{\theta_s D_s}{K_s} \ln u. \tag{4}$$

The angle α may be spatially distributed, but is assumed to be constant in this paper. There exist two contrasting cases on arrangement of the sheets, which are the horizontal ($\alpha = 0$) and vertical cases ($\alpha = \pm 0.5\pi$). The advection term of (1) vanishes in the horizontal case because of the equality $\sin \alpha = 0$. Hereafter, “ \cdot ” representing non-dimensional variables are omitted from the variables for the sake of simplicity of description.

Degenerate advection and diffusion terms of (1) possibly serve as severe mathematical and computational difficulties at the point of degeneration ($u = 0$) in particular. This paper mitigates the degeneration with a regularization technique [50], which modifies (1) as

$$\frac{\partial u}{\partial t} = \frac{\partial}{\partial x} \left((m-p)[h_\varepsilon(u)]^{m-p-1} \frac{\partial u}{\partial x} \right) + \sin \alpha \frac{\partial}{\partial x} \left([h_\varepsilon(u)]^{m-1} u \right) - E_s u^q \tag{5}$$

with the regularization kernel $h_\varepsilon(u) = \sqrt{u^2 + \varepsilon^2}$ ($\geq \varepsilon$) and a small positive constant ε ($= 10^{-6}$ in this paper), which completely rules out the degeneration. The diffusion coefficient in (5) is entirely positive over the domain where the PME (1) is considered. The regularized extended PME (5) can be written in the flux form as

$$\frac{\partial u}{\partial t} + \frac{\partial F}{\partial x} = -E_s u^q \tag{6}$$

with the flux $F = F(u)$ given by

$$F = -(m-p)[h_\varepsilon(u)]^{m-p-1} \frac{\partial u}{\partial x} - \sin \alpha [h_\varepsilon(u)]^{m-1} u. \tag{7}$$

Convergence of numerical solutions subject to the regularization to the exact solutions, at least practically, is demonstrated in Section 4, where utilizing sufficiently small regularization parameter does not significantly affects the computational results. This is possibly because the computational errors in the spatial and temporal discretization dominate that due to the regularization. It should be remarked that a similar regularization technique has already been successfully applied to nonlinear advection-diffusion equations with both mathematical and numerical analyzes [63]. Mathematically rigorous analysis of the regularization method for the PME, which would be more difficult to perform, is beyond the scope of this paper and will be addressed elsewhere.

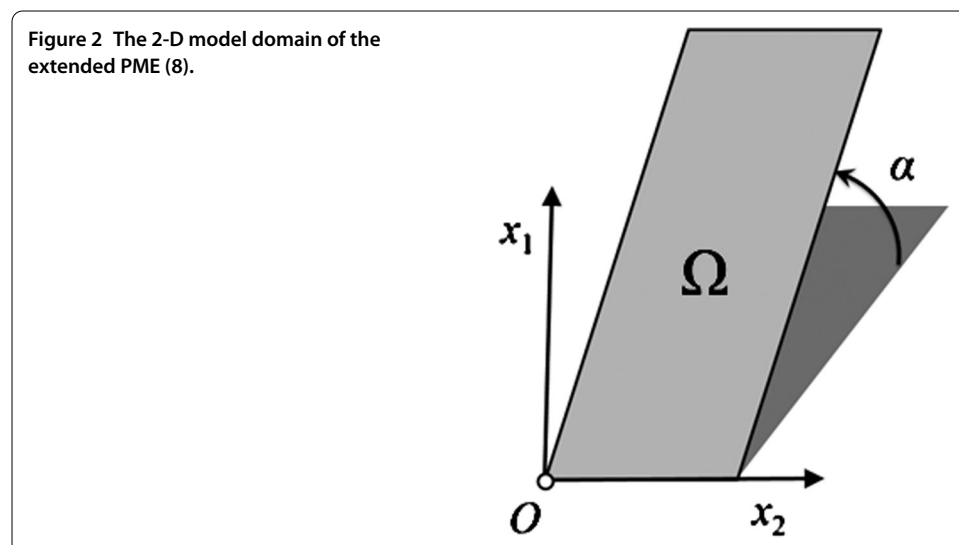
2.2 2-D extended porous medium equation

The 2-D extended PME, which is a 2-D counterpart of the 1-D model (1), is presented. This model is necessary for simulating essentially 2-D moisture dynamics in inclined fibrous sheets, such that an application of the 1-D model is inadequate. The inclination angle is again denoted by α , which is typically horizontal ($\alpha = 0$) or vertical ($\alpha = \pm 0.5\pi$) of the sheet. The 2-D x_1 - x_2 Cartesian coordinates is taken over the surface of the sheet, which is identified with a 2-D flat domain Ω as depicted in Figure 2. It is assumed for the sake of simplicity of description that the sheet is horizontal on the x_2 -direction. Under this assumption, the 2-D extended PME that governs the saturation $u = u(t, x_1, x_2)$ in Ω is presented as

$$\begin{aligned} \frac{\partial u}{\partial t} = & \frac{\partial}{\partial x_1} \left((m-p)u^{m-p-1} \frac{\partial u}{\partial x_1} \right) \\ & + \frac{\partial}{\partial x_2} \left((m-p)u^{m-p-1} \frac{\partial u}{\partial x_2} \right) + \sin \alpha \frac{\partial}{\partial x_1} (u^{m-1}u) - E_s u^q \end{aligned} \tag{8}$$

subject to appropriate initial and boundary conditions. The regularized counterpart of (8) is given following (5) as

$$\begin{aligned} \frac{\partial u}{\partial t} = & \frac{\partial}{\partial x_1} \left((m-p)[h_\varepsilon(u)]^{m-p-1} \frac{\partial u}{\partial x_1} \right) + \frac{\partial}{\partial x_2} \left((m-p)[h_\varepsilon(u)]^{m-p-1} \frac{\partial u}{\partial x_2} \right) \\ & + \sin \alpha \frac{\partial}{\partial x_1} ([h_\varepsilon(u)]^{m-1}u) - E_s u^q \end{aligned} \tag{9}$$



to practically mitigate the degeneration. As for the 1-D model, (9) can be written in the flux form as

$$\frac{\partial u}{\partial t} + \frac{\partial F_1}{\partial x_1} + \frac{\partial F_2}{\partial x_2} = -E_s u^q \tag{10}$$

with the couple of fluxes (F_1, F_2) given by

$$\begin{pmatrix} F_1 \\ F_2 \end{pmatrix} = \begin{pmatrix} -(m-p)[h_\varepsilon(u)]^{m-p-1} \frac{\partial u}{\partial x_1} - \sin \alpha [h_\varepsilon(u)]^{m-1} u \\ -(m-p)[h_\varepsilon(u)]^{m-p-1} \frac{\partial u}{\partial x_2} \end{pmatrix}, \tag{11}$$

which is a more suitable expression for application of and FVM.

Finally, in this section, remarks on boundary conditions to be supplemented to the 2-D extended PME and its regularized counterpart are provided with particular emphasis on the wetting process. From a mathematical viewpoint, at least some boundary conditions should be supplemented to these PMEs in general, since they are partial differential equations of the parabolic-type, although with possible degeneration of the coefficients. From a physical view point, a reasonable boundary condition for simulating a wetting process where a part of the boundary of the domain $(\partial\Omega_W)$ touches liquid water is the Dirichlet boundary condition $u = 1$ meaning that the boundary $\partial\Omega_W$ is fully-wet. Of course, it is theoretically possible to specify the net flux $\mathbf{F} \cdot \mathbf{n}$ on $\partial\Omega_W$, but directly measuring the flux is, at least to our experience, technically not easy. On the other part of the boundary, a simple and appropriate boundary condition is the no-flux condition $\mathbf{F} \cdot \mathbf{n} = 0$ where the inner product between the flux vector \mathbf{F} and the outward boundary normal vector \mathbf{n} vanishes. This boundary condition represents that no liquid water escapes from the boundary, which is a reasonable assumption for moisture dynamics with evaporation as focused on in this paper later.

3 2-D dual-finite volume method

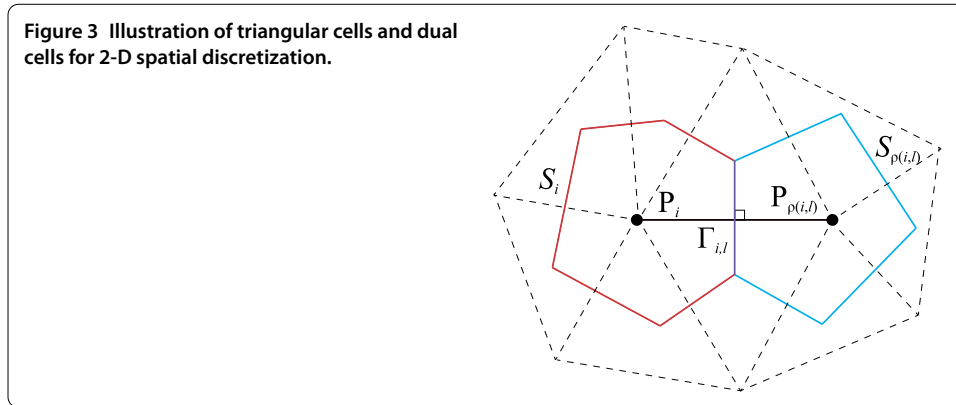
The discretization procedure of the 2-D DFVM is explained in this section.

3.1 Spatial discretization

The 2-D domain Ω is divided into triangular (regular) cells in the usual conforming manner. The cells and the nodes are indexed with the natural numbers. The total numbers of the regular cells and nodes are denoted by N_e and N_n , respectively. The i th node is denoted by P_i . The number of nodes directly connected to the node P_i is denoted by $\tau(i)$ and the l th of them is denoted by the $\rho(i, l)$ th node $P_{\rho(i,l)}$. The length of the edge $P_i P_{\rho(i,l)}$ is denoted by $d_{i,l}$. A dual cell associated with the node P_i is denoted by S_i , which is defined as the conventional 2-D Voronoi cell [64]

$$S_i = \bigcup_{l=1}^{\tau(i)} S_{i,l} = \bigcup_{l=1}^{\tau(i)} \{ \mathbf{x} \mid \text{dist}(\mathbf{x}, P_i) < \text{dist}(\mathbf{x}, P_{\rho(i,l)}) \}, \tag{12}$$

where $\text{dist}(\cdot, \cdot)$ represents the conventional distance function between a couple of points located in the domain Ω . Figure 3 illustrates the 2-D computational cells used in this paper. The area of the dual cell S_i is denoted by $|S_i|$. The length of the outer perimeter of the sub-cell $S_{i,l}$ of the dual cell S_i is denoted by $L_{i,l}$. The unknown u is attributed to the dual cells (or equivalently to the nodes).



3.2 Operator-splitting algorithm

The regularized counterpart (9) is regarded as an advection-diffusion-decay equation having solution-dependent coefficients, which are discretized fully explicitly at each time step. The 2-D DFVM thus avoids using nonlinear iteration methods such as the Newton and Picard algorithms to realize a simpler and more easily implementable numerical algorithm. An operator-splitting algorithm analogous to that of Li et al. [59] specialized for (9) is incorporated into the 2-D DFVM, so that numerical instability due to nonlinearity of the evaporation term is avoided. This approach has successfully been used for conservation laws with nonlinear source terms [65, 66]. The time increment at each time step is denoted as Δt and the partial differential operators defining the advection and diffusion terms of (9) as P_{AD} and that for the evaporation term as P_E : namely,

$$\begin{aligned}
 P_{AD}\phi &= \frac{\partial}{\partial x_1} \left((m-p)[h_\varepsilon(\phi)]^{m-p-1} \frac{\partial \phi}{\partial x_1} \right) \\
 &\quad + \frac{\partial}{\partial x_2} \left((m-p)[h_\varepsilon(\phi)]^{m-p-1} \frac{\partial \phi}{\partial x_2} \right) + \sin \alpha \frac{\partial}{\partial x_1} ([h_\varepsilon(\phi)]^{m-1} \phi) \quad \text{and} \quad (13) \\
 P_E\phi &= -E_s\phi^q
 \end{aligned}$$

for generic $\phi = \phi(x_1, x_2)$. The 2-D DFVM discretizes (9) at each time step as

$$u^{(k+1)} = \exp(0.5\Delta t P_E) \exp(\Delta t P_{AD}) \exp(0.5\Delta t P_E) u^{(k)}, \quad (14)$$

where $u^{(k)}$ represents the numerical solution at the k th time step. Although the 2-D DFVM is unconditionally stable for linear advection-diffusion equations, preliminary computation showed that it is not the case for the extended PME if Δt is too large. The reason of this issue would be the loss of ellipticity of the discretized system as already implied in Pop et al. [67]. This drawback would be overcome if an implicit treatment of the coefficients is used, which will be addressed in future research. Discretization procedure of the two sub-steps is explained below.

3.3 Evaporation sub-step

At an evaporation sub-step, the equation to be solved at each node is expressed as the ordinary differential equation (ODE)

$$\frac{\partial u}{\partial t} = -E_s u^q. \quad (15)$$

Let U_i be the nodal value of the numerical solution at the previous time step or that at the end of the previous advection-diffusion sub-step at the i th node. Starting from the formal initial condition U_i at the time t_0 , (15) with $t > t_0$ follows

$$u_i(t) = \begin{cases} (\max\{0, \phi_i(U_i, t, t_0)\})^{\frac{1}{1-q}} & (0 < q < 1) \\ U_i \exp(-E_s(t - t_0)) & (q = 1) \end{cases} \tag{16}$$

with

$$\phi_i(u, t, t_0) = u^{1-q} - (1 - q)E_s(t - t_0) \tag{17}$$

for $u \in \mathbb{R}^+$. By (16), the first evaporation sub-step at the k th time step for the i th node is

$$u_i^* = \exp_d(0.5\Delta t P_E)u^{(k)} \tag{18}$$

with

$$\exp_d(0.5\Delta t P_E)u_i^{(k)} = \begin{cases} (\max\{0, \phi_i(u_i^{(k)}, t + 0.5\Delta t, t)\})^{\frac{1}{1-q}} & (0 < q < 1) \\ u_i^{(k)} \exp(-E_s 0.5\Delta t) & (q = 1), \end{cases} \tag{19}$$

where u_i^* represents the updated nodal value, which is used as the initial condition of the advection-diffusion sub-step. The updated nodal value at the i th node just after the advection-diffusion sub-step is denoted as u_i^{**} . The second evaporation sub-step is then expressed as

$$u^{(k+1)} = \exp_d(0.5\Delta t P_E)u_i^{**} \tag{20}$$

with

$$\exp_d(0.5\Delta t P_E)u_i^{**} = \begin{cases} (\max\{0, \phi_i(u_i^{**}, t + 0.5\Delta t, t)\})^{\frac{1}{1-q}} & (0 < q < 1) \\ u_i^{**} \exp(-0.5E_s\Delta t) & (q = 1). \end{cases} \tag{21}$$

No restriction on Δt has to be imposed for each evaporation sub-step because the temporal integration on the evaporation term is carried out with the analytical solutions.

3.4 Advection-diffusion sub-step

At the advection-diffusion sub-step, the equation to be solved is given by

$$\frac{\partial u}{\partial t} + \frac{\partial F_1}{\partial x_1} + \frac{\partial F_2}{\partial x_2} = 0. \tag{22}$$

A finite volume discretization is applied to (22) as explained below.

3.4.1 Finite volume formulation

Integrating the (22) in the dual cell S_i with the application of the Gauss-Green theorem yields

$$\frac{\partial}{\partial t} \int_{S_i} u \, ds + \sum_{l=1}^{\tau(i)} L_{i,l} F_{i,l} = 0, \tag{23}$$

where $F_{i,l}$ is the numerical flux to be evaluated on the cell face between the dual cells S_i and $S_{\rho(i,l)}$. The first term in the left hand-side of (23) is evaluated as

$$\frac{\partial}{\partial t} \int_{S_i} u \, dx \approx |S_i| \frac{du_i}{dt}. \tag{24}$$

The numerical flux $F_{i,l}$ is evaluated with a fitting technique, which uses the analytical solution \tilde{u} of the two-point boundary value problem

$$\frac{\partial}{\partial s} \left(b_{\rho(i,l)} \tilde{u} - a_{\rho(i,l)} \frac{\partial \tilde{u}}{\partial s} \right) = 0 \tag{25}$$

along the edge $P_i P_{\rho(i,l)}$ with the local 1-D coordinate s taken from P_i to $P_{\rho(i,l)}$ and the boundary conditions

$$\tilde{u}(x_i) = u_i, \quad \tilde{u}(x_{\rho(i,l)}) = u_{\rho(i,l)} \tag{26}$$

with

$$a_{\rho(i,l)} = (m - p) [h_\varepsilon(\overline{u_{\rho(i,l)}})]^{m-p-1} \quad \text{and} \quad b_{\rho(i,l)} = -\sin \alpha [h_\varepsilon(\overline{u_{\rho(i,l)}})]^{m-1} n_{1,\rho(i,l)}, \tag{27}$$

where $\overline{u_{\rho(i,l)}}$ represents the value of u on the edge $P_i P_{\rho(i,l)}$ that is specified later and $n_{1,\rho(i,l)}$ is the x_1 -component of the unit normal vector $(n_{1,\rho(i,l)}, n_{2,\rho(i,l)})$ having the same direction with the vector $\overrightarrow{P_i P_{\rho(i,l)}}$. The analytical solution \tilde{u} is obtained as

$$\tilde{u} = \frac{\exp(p_{i,l}) u_i - u_{\rho(i,l)}}{\exp(p_{i,l}) - 1} + \frac{u_{\rho(i,l)} - u_i}{\exp(p_{i,l}) - 1} \exp\left(\frac{b_{\rho(i,l)}}{a_{\rho(i,l)}}(s - s_i)\right), \tag{28}$$

which is used for directly evaluating the numerical flux $F_{i,l}$ as

$$\begin{aligned} F_{i,l} &= b_{\rho(i,l)} \tilde{u} - a_{\rho(i,l)} \frac{\partial \tilde{u}}{\partial s} \\ &= \frac{(m - p) n_{1,\rho(i,l)} d_{i,l}}{d_{i,l}} [h_\varepsilon(\overline{u_{\rho(i,l)}})]^{m-p-1} p_{i,l} \frac{\exp(p_{i,l}) u_i - u_{\rho(i,l)}}{\exp(p_{i,l}) - 1}, \end{aligned} \tag{29}$$

with the local Peclet number

$$p_{i,l} = -\frac{n_{1,\rho(i,l)} d_{i,l} \sin \alpha}{m - p} h_\varepsilon(\overline{u_{\rho(i,l)}})^p. \tag{30}$$

The numerical flux $F_{i,l}$ is fully specified if the value of $\overline{u_{\rho(i,l)}}$ is evaluated. A remarkable point of the 2-D DFVM is that the Peclet number $p_{i,l}$ is independent of u when $p = 0$: By (30), $p_{i,l}$ with $p = 0$ is expressed as

$$p_{i,l} = -\frac{n_{1,\rho(i,l)} d_{i,l} \sin \alpha}{m}. \tag{31}$$

This property help establish an isotonic numerical flux as presented below.

3.4.2 Numerical flux

The value of $\overline{u_{\rho(i,l)}}$ is specified to determine $F_{i,l}$. The three evaluation schemes for $\overline{u_{\rho(i,l)}}$ are presented in this paper, which are the central (CE) scheme, fully-upwind (FU) scheme, and the isotone (IS) scheme. The CE and FU scheme have been used in Fuhrmann and Langmach [49], and the IS scheme is a new numerical method proposed in this paper. The approximation $\varepsilon = 0$ is used in this and next sections because it is assumed to be a sufficiently small positive constant such that it does not significantly affect accuracy of numerical solutions.

The CE and FU schemes evaluate $\overline{u_{\rho(i,l)}}$ as

$$\overline{u_{\rho(i,l)}} = \frac{1}{2}(u_i + u_{\rho(i,l)}) \tag{32}$$

and

$$\overline{u_{\rho(i,l)}} = \max(u_i, u_{\rho(i,l)}), \tag{33}$$

respectively.

The concept of isotonicity is presented in this sub-section for proposing an isotonic numerical flux suited to solving the extended PME. The numerical flux is regarded as a bi-variate function of the non-negative parameters $\lambda, \mu \geq 0$ as

$$F_{i,l} = \tilde{F}_{i,l}(\lambda, \mu)|_{\lambda=u_i, \mu=u_{\rho(i,l)}} \tag{34}$$

with

$$\tilde{F}_{i,l}(\lambda, \mu) = \frac{mn_{1,\rho(i,l)}p_{i,l}}{d_{i,l}} (\overline{u_{\rho(i,l)}}(\lambda, \mu))^{m-1} \frac{\exp(p_{i,l})u_i - u_{\rho(i,l)}}{\exp(p_{i,l}) - 1}. \tag{35}$$

The numerical flux $F_{i,l}$ is said to be isotone if both

$$n_{1,\rho(i,l)} \frac{\partial \tilde{F}_{i,l}}{\partial \lambda} \geq 0 \tag{36}$$

and

$$-n_{1,\rho(i,l)} \frac{\partial \tilde{F}_{i,l}}{\partial \mu} \geq 0 \tag{37}$$

for arbitrary $\lambda, \mu \geq 0$ [49]. The value of $\overline{u_{\rho(i,l)}}$ should be determined so that both (36) and (37) are satisfied; however, analytically finding such $\overline{u_{\rho(i,l)}}$ in generic cases is difficult because of the nonlinearity of $\tilde{F}_{i,l}$. An exceptional case is that with $p = 0$ where the analytical expression of $\overline{u_{\rho(i,l)}}$ is found as demonstrated in the next subsection.

3.4.3 Isotonicity on the CE scheme

The CE scheme possibly gives unphysical (negative) numerical solutions because it does not comply with (36) and (37) even with the absence of advection term [32].

3.4.4 Isotonicity on the FU scheme

The FU scheme can potentially mitigate such computational difficulty but has excessive numerical diffusion. In addition, FU scheme with the 2-D DFVM is not isotone as shown below. The quantities $n_{1,\rho(i,l)} \frac{\partial \tilde{F}_{i,l}}{\partial \lambda}$ and $-n_{1,\rho(i,l)} \frac{\partial \tilde{F}_{i,l}}{\partial \mu}$ are calculated for $\lambda \geq \mu \geq 0$ with the FU scheme as

$$\begin{aligned} n_{1,\rho(i,l)} \frac{\partial \tilde{F}_{i,l}}{\partial \lambda} &= \frac{\partial}{\partial \lambda} \left[\frac{mp_{i,l}}{d_{i,l}} \lambda^{m-1} \frac{\exp(p_{i,l})\lambda - \mu}{\exp(p_{i,l}) - 1} \right] \\ &= \frac{m}{d_{i,l}} \frac{p_{i,l}}{\exp(p_{i,l}) - 1} (m \exp(p_{i,l})\lambda - (m-1)\mu) \lambda^{m-2} \end{aligned} \tag{38}$$

and

$$\begin{aligned} -n_{1,\rho(i,l)} \frac{\partial \tilde{F}_{i,l}}{\partial \mu} &= \frac{\partial}{\partial \mu} \left[\frac{mp_{i,l}}{d_{i,l}} \lambda^{m-1} \frac{\mu - \exp(p_{i,l})\lambda}{\exp(p_{i,l}) - 1} \right] \\ &= \frac{m}{d_{i,l}} \frac{p_{i,l}}{\exp(p_{i,l}) - 1} \lambda^{m-1} \\ &\geq 0, \end{aligned} \tag{39}$$

respectively. Similarly, for $\mu \geq \lambda \geq 0$ with the FU scheme, the inequalities are calculated as

$$\begin{aligned} n_{1,\rho(i,l)} \frac{\partial \tilde{F}_{i,l}}{\partial \lambda} &= \frac{\partial}{\partial \lambda} \left[\frac{mp_{i,l}}{d_{i,l}} \mu^{m-1} \frac{\exp(p_{i,l})\lambda - \mu}{\exp(p_{i,l}) - 1} \right] \\ &= \frac{m}{d_{i,l}} \frac{p_{i,l} \exp(p_{i,l})}{\exp(p_{i,l}) - 1} \mu^{m-1} \\ &\geq 0 \end{aligned} \tag{40}$$

and

$$\begin{aligned} -n_{1,\rho(i,l)} \frac{\partial \tilde{F}_{i,l}}{\partial \mu} &= \frac{\partial}{\partial \mu} \left[\frac{mp_{i,l}}{d_{i,l}} \mu^{m-1} \frac{\mu - \exp(p_{i,l})\lambda}{\exp(p_{i,l}) - 1} \right] \\ &= \frac{m}{d_{i,l}} \frac{p_{i,l}}{\exp(p_{i,l}) - 1} [m\mu - (m-1)\exp(p_{i,l})\lambda] \mu^{m-2}, \end{aligned} \tag{41}$$

respectively. By (38), (36) follows if

$$\exp(p_{i,l}) - \frac{m-1}{m} \geq 0. \tag{42}$$

Similarly, by (41), (37) follows if

$$\exp(-p_{i,l}) - \frac{m-1}{m} \geq 0. \tag{43}$$

Thus, both (36) and (37) are true if

$$\frac{m-1}{m} \leq \exp(p_{i,l}) \leq \frac{m}{m-1}, \tag{44}$$

demonstrating that the FU scheme is not isotone when the condition (44) is violated, which is true when the advection is dominant.

3.4.5 Isotonicity on the IS scheme

A new evaluation scheme of the numerical flux, the IS scheme, is presented as a possible alternative to the CE and FU schemes. Assuming $p = 0$ for mathematical tractability, the IS scheme is expressed as

$$\overline{u_{\rho(i,l)}} = \begin{cases} u_i & (\text{if } \exp(p_{i,l})u_i - u_{\rho(i,l)} \geq 0) \\ u_{\rho(i,l)} & (\text{otherwise}). \end{cases} \tag{45}$$

By (36) and (37), isotonicity of the IS scheme follows for $\exp(p_{i,l})\lambda - \mu \geq 0$ as

$$\begin{aligned} n_{1,\rho(i,l)} \frac{\partial \tilde{F}_{i,l}}{\partial \lambda} &= \frac{m}{d_{i,l}} \frac{p_{i,l}}{\exp(p_{i,l}) - 1} \lambda^{m-2} (m \exp(p_{i,l})\lambda - (m-1)\mu) \\ &\geq \frac{m}{d_{i,l}} \frac{p_{i,l}}{\exp(p_{i,l}) - 1} \lambda^{m-2} (m \exp(p_{i,l})\lambda - (m-1)\exp(p_{i,l})\lambda) \\ &= \frac{m}{d_{i,l}} \frac{p_{i,l} \exp(p_{i,l})}{\exp(p_{i,l}) - 1} \lambda^{m-1} \\ &\geq 0 \end{aligned} \tag{46}$$

that verifies (36). The scheme for $\exp(p_{i,l})\lambda - \mu \geq 0$ verifies (37) as

$$-n_{1,\rho(i,l)} \frac{\partial \tilde{F}_{i,l}}{\partial \mu} = \frac{m}{d_{i,l}} \frac{p_{i,l}}{\exp(p_{i,l}) - 1} \lambda^{m-1} \geq 0. \tag{47}$$

The proof of the isotonicity of the IS scheme for $\exp(p_{i,l})\lambda - \mu < 0$ proceeds in an essentially similar way since

$$n_{1,\rho(i,l)} \frac{\partial \tilde{F}_{i,l}}{\partial \lambda} = \frac{m}{d_{i,l}} \frac{p_{i,l} \exp(p_{i,l})}{\exp(p_{i,l}) - 1} \mu^{m-1} \geq 0 \tag{48}$$

and

$$\begin{aligned} -n_{1,\rho(i,l)} \frac{\partial \tilde{F}_{i,l}}{\partial \mu} &= \frac{\partial}{\partial \mu} \left[\frac{mp_{i,l}}{d_{i,l}} \mu^{m-1} \frac{\mu - \exp(p_{i,l})\lambda}{\exp(p_{i,l}) - 1} \right] \\ &= \frac{mp_{i,l}}{d_{i,l}} \frac{m\mu - (m-1)\exp(p_{i,l})\lambda}{\exp(p_{i,l}) - 1} \mu^{m-2} \\ &> \frac{m}{d_{i,l}} \frac{p_{i,l}}{\exp(p_{i,l}) - 1} \mu^{m-1} \\ &\geq 0. \end{aligned} \tag{49}$$

(40), (46), and (47) prove that the IS scheme is isotone. In this paper, for the sake of simplicity of analysis, the FU scheme is used for the 2-D model when $p > 0$. This is because the analytical condition for choosing $\overline{u_{\rho(i,l)}}$ as in (45) is not available. Nevertheless, for small p such that $m \gg p$ the IS scheme is expected to be not completely but nearly isotone. The condition $m \gg p$ is actually satisfied for a non-woven fibrous sheet examined in Section 4.

3.4.6 Temporal integration

Assembling (23) for every node yields the system of linear ODEs. The 2-D DFVM finally yields the system of linear ODEs

$$\frac{d\mathbf{u}}{dt} = \Xi\mathbf{u} + \xi, \tag{50}$$

where $\mathbf{u} = [u_i]$ is the N_n -dimensional solution vector, $\Xi = [\Xi_{i,k}]$ is the $N_n \times N_n$ -dimensional matrix arising from the spatial discretization, and $\xi = [\xi_i]$ is the N_n -dimensional vector independent of \mathbf{u} . The boundary conditions, if necessary, are included in ξ . The system of ODEs (50) is temporally integrated with the θ -method [68]. This paper specifies θ as 1 (Fully implicit scheme). In the 2-D DFVM, the temporal integration of the advection-diffusion sub step is then expressed as

$$\mathbf{u}^{**} = (I - \Xi\Delta t)^{-1}(\mathbf{u}^* + \xi\Delta t), \tag{51}$$

where I is the $N_n \times N_n$ -dimensional identity matrix and the vectors \mathbf{u}^{**} and \mathbf{u}^* are given by $\mathbf{u}^* = [u_i^*]$ and $\mathbf{u}^{**} = [u_i^{**}]$, respectively. The inversion of the matrix $I - \Xi$ is justified because of the positivity conditions of the spatial discretization in the 2-D DFVM as proved in Yoshioka and Unami [51]. The linear system is numerically solved with the conventional Gauss-Seidel method whose iteration is terminated until the absolute value of the difference of nodal values between before and after an updating is smaller than 10^{-8} for every node.

4 Application

4.1 Test cases

The 2-D DFVM is applied to a series of test cases for its verification of accuracy and stability. Note that the aim of these test cases is not comparing the 2-D DFVM with other methods but to confirm its satisfactory convergence to analytical solutions, since the purpose of this paper is establishment of a mathematical model and a simple numerical method that can reasonably simulate the 2-D moisture dynamics. In each test case, the independent variables are appropriately scaled without the loss of generality. The 2-D DFVM is developed in a standard C++ environment. Each unstructured triangular computational mesh in what follows has been generated with free software VORO Ver. 3.17 (available at <http://www32.ocn.ne.jp/~yss/voro.html>). The 2-D DFVM with the operator splitting technique is expected to perform first-order accuracy in time according to Li et al. [59]. Note that using the Crank-Nicolson scheme ($\theta = 0.5$) in the temporal integration of the advection-diffusion sub-step yields oscillatory numerical solutions in the test cases examined below. The exact solutions in some test cases are partially $u > 1$, which is physically invalid. These test cases therefore solely concern computational accuracy of the 2-D DFVM and do not discuss physical meaning of the solutions.

4.1.1 Test 1: Barenblatt problem

This is a classical, radially symmetric weak solution to the conventional PME that has a sharp and non-smooth profile [69]. The PME to be solved is given by

$$\frac{\partial u}{\partial t} = \left(\frac{\partial^2}{\partial x_1^2} + \frac{\partial^2}{\partial x_2^2} \right) u^m \quad \text{in } \mathbb{R}^2 \tag{52}$$

whose exact solution, the Barenblatt solution, is expressed for $t > 0$ as

$$u_{Ba}(t, x_1, x_2) = \max \left\{ 0, \frac{1}{t^m} \left[1 - \frac{(m-1)(x_1^2 + x_2^2)}{4t^m} \right]^{\frac{1}{m-1}} \right\}. \tag{53}$$

A series of structured (square) dual grid with the resolution of 32×32 , 64×64 , 128×128 , and 256×256 are examined and the numerical solutions are compared with the exact solution (53) for $m = 2, 3$, and 4 and the convergence rate was estimated for each m . The time increment Δt is set as 0.001 throughout this test case. The initial condition is set as $u(0, x_1, x_2) = u_{Ba}(0.001, x_1, x_2)$ to avoid the deltaic singularity of the initial condition at the time $t = 0$ of u_{Ba} . The computational domain is set as the square $(-5, 5) \times (-5, 5)$ where the support of the exact solution does not touch its boundary at least at the time $t = 0.200$ where the exact and numerical solutions are compared. The conventional nodal l^2 error norm Er between exact u_{exact} and numerical solutions $u_{numerical}$, which is defined as

$$Er = \sqrt{\frac{1}{N_n} \sum_{i=1}^{N_n} (u_{exact} - u_{numerical})^2} \tag{54}$$

is used as an error metric throughout this paper. The reason of using structured meshes is to verify exact symmetry of the numerical solutions with respect to the x_1 - and x_2 -axis that the meshes have. The focus of this test case is on accuracy of the scheme in space rather than in time. The exact and numerical solutions are compared at $t = 0.15$.

Figure 4(a) through 4(c) compare the numerical and exact solutions for $m = 2, 3$, and 4 with the spatial resolution of 128×128 . Table 1 summarizes the error norms and convergence rates. The numerical solutions are certainly axially symmetric but not radially symmetric because of using the structured grid that does not have radial symmetry. The radial symmetry is recovered and the front position is more accurately captured as the mesh is refined. The computational results show that the order of convergence of the 2-D DFVM degrades as the parameter m for the nonlinearity increases. The order of convergence is almost one for each m . Qualitatively similar computational results have been obtained for $m = O(10^0)$.

4.1.2 Test 2: steady problem with evaporation

This second test considers water infiltration from one side ($x_1 = 0$) of a horizontal sheet ($\alpha = 0$ and $p = 0$) in evaporative environment [4]. The domain is set as the unit square $(0, 1) \times (0, 1)$. Assuming that $u = 1$ on the boundary $x_1 = 0$, an elementary calculation shows that the steady solution to this test case is

$$u(x_1, x_2) = \max \left\{ \left(1 - (m-q) \sqrt{\frac{E_s}{2m(m+q)} x_1} \right)^{\frac{2}{m-q}}, 0 \right\}, \tag{55}$$

which is homogenous in the x_2 -direction. The function in the exact solution is cut to 0 if it becomes negative as in the right-hand side of (55). The support of the exact solution is bounded when $m > q$. This analytical solution is a weak solution since it is continuous but not differentiable at the free boundary. The focus of this test case is to see ability of the 2-D DFVM to capture the steady state solutions having bounded supports. The time

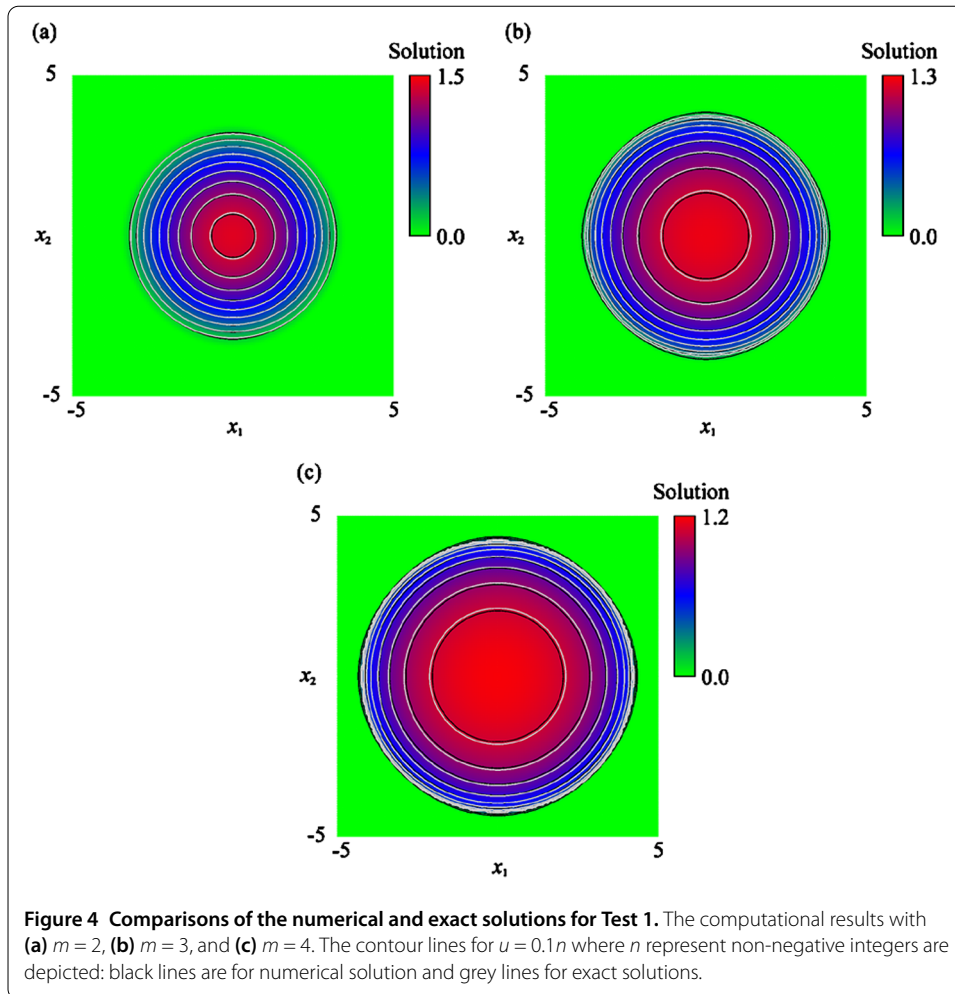


Table 1 Computed error norms and the order of convergence for Test 1

Mesh	Error norm			Order of convergence in space		
	$m = 2$	$m = 3$	$m = 4$	$m = 2$	$m = 3$	$m = 4$
32×32	3.66E-02	6.29E-02	7.69E-02			
64×64	2.12E-02	4.12E-02	5.70E-02	7.88E-01	6.10E-01	4.32E-01
128×128	8.54E-03	2.22E-02	3.40E-02	1.31E+00	8.92E-01	7.45E-01
256×256	3.85E-03	1.25E-02	2.28E-02	1.15E+00	8.29E-01	5.77E-01

increment is set as $\Delta t = 0.001$. Steady numerical solutions are computed starting from the initial guess $u = 0$ over the computational domain where the homogenous Neumann condition is specified on the boundaries $x_2 = 0$, $x_2 = 1$, and $x_1 = 1$; the last one does not affect computational results since the numerical solutions almost vanish near $x_1 = 1$. The parameters E_s , m , and q can be chosen such that the support of the exact solution (55) becomes $[0, 0.5]$. The parameter q for the evaporation term is fixed to 0.01, and examined $m = 3$, so that $E_s = 8.08$. The final time of computation is empirically set as $t = 5$ at which the numerical solutions are observed to be sufficiently close to steady state. A series of structured (square) dual grids with the resolution of 32×16 , 64×16 , and 128×16 are examined. In addition, the time increment of 0.01, 0.001, and 0.0001 are examined.

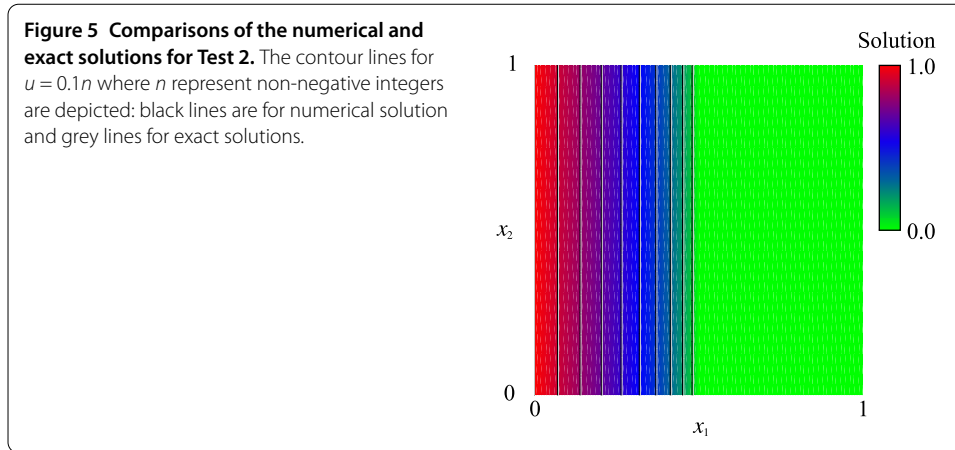


Table 2 Computed error norms and the order of convergence for Test 2

Time increment Δt	Error norm			Order of convergence in time		
	32 x 16	64 x 16	128 x 16	32 x 16	64 x 16	128 x 16
0.01	5.04E-02	5.77E-02	6.05E-02			
0.001	6.35E-03	5.01E-03	5.51E-03	9.00E-01	1.06E+00	1.04E+00
0.0001	1.29E-02	5.65E-03	2.31E-03	-3.08E-01	-5.22E-02	3.78E-01

Figure 5 compares the numerical and exact solutions for the spatial and temporal resolution of 128×128 and $\Delta t = 0.001$. Table 2 summarizes the error norms and convergence rates in time. Table 2 implies that choosing too small Δt for a given computational mesh would not be effective. This is considered due to that the front position of the solution is sensitive to spatial resolution rather than the temporal resolution. This computational result suggests employing fine spatial resolution rather than fine temporal resolution would be effective for analyzing steady problems with the support. The computational result also suggests that both space and time resolution should be fine for computing steady solutions having the source term, which is considered to be due to dependence of the numerical solution on Δt through the proposed operator-splitting process.

4.1.3 Test 3: travelling wave solution

The travelling wave solutions available in Nasseri et al. [70] are used for examining the present DFVM against the 2-D extended PME without the source term. A particular emphasis is put on a comparison of the performances of the FU and IS schemes for evaluation of the numerical fluxes. The equation to be discretized is the extended PME for $\alpha = 0.5\pi$ without the evaporation term and $p = 0$ whose exact solution is expressed as

$$u = \left[\frac{c}{2} \left\{ 1 + \tanh \left(-\frac{m-1}{2mD} (x_2 - ct) \right) \right\} \right]^{\frac{-1}{m-1}}, \tag{56}$$

where c is set to be 1, m is fixed to 3 in the present case, and the diffusion coefficient $D = 0.25$ is multiplied by the second-order partial differential terms. This problem is an initial and boundary value problem of a nonlinear advection-diffusion equation where the source term is absent whose focus is to assess its ability of capturing travelling wave-type solutions that often arise in describing moisture dynamics in porous media [71, 72].

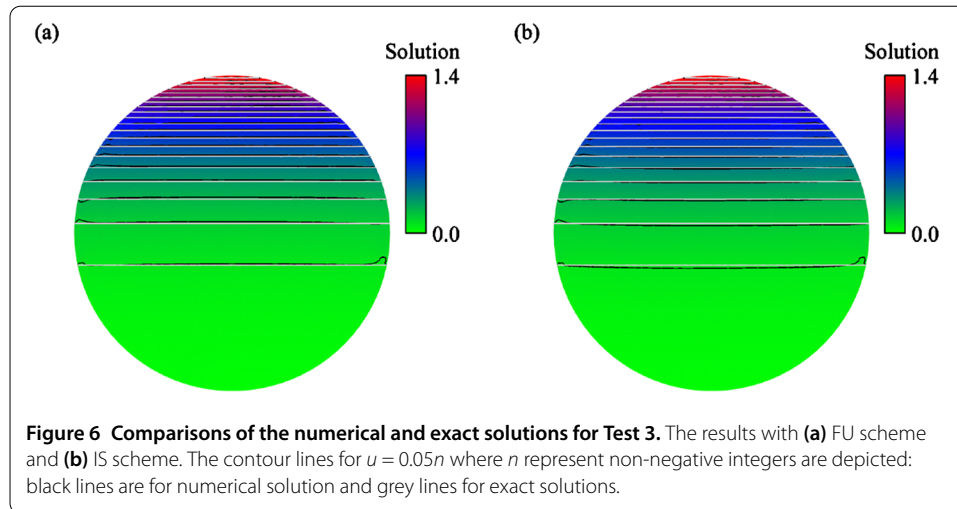


Table 3 Computed error norms and the order of convergence for Test 3

Mesh	Error norm		Order of convergence in space	
	FU scheme	IS scheme	FU scheme	IS scheme
348 cells	6.95E-03	5.11E-03		
1,296 cells	4.29E-03	3.39E-03	6.98E-01	5.92E-01
4,949 cells	1.67E-03	9.80E-04	1.36E+00	1.79E+00
19,565 cells	7.61E-04	5.96E-04	1.14E+00	7.17E-01

Since the present DFVM reduces to the conventional upwind FVM for small diffusion coefficient, its expected order of accuracy in space is one. The same computational meshes with the previous test cases and the additional, finer mesh with 38,588 triangular cells and 19,565 dual cells are examined. The numerical and exact solutions are compared at the time $t = 1$. The time increment Δt is set to be 0.0001, which is found to be sufficiently small to for assessing computational accuracy in space of the FU and IS schemes.

Figure 6(a) and 6(b) compare the numerical and exact solutions to this test case with the second finest mesh for the 2-D DFVM with the FU and IS schemes, respectively. Table 3 compares the error norms for the present test case with the FU and IS schemes, showing that the convergence order of the both of the schemes are almost one. It is also shown that the numerical solutions with the IS scheme have several tens present have smaller errors than those with the FU scheme except for the finest mesh. There is no significant qualitative difference between the obtained numerical solutions with the FU and IS schemes. The results indicate that the IS scheme performs slightly better than the FU scheme for the traveling wave-type solutions.

4.2 Demonstrative application

A demonstrative application example of the 2-D (regularized) extended PME and the 2-D DFVM to simulating moisture dynamics in an existing non-woven fibrous sheet is presented in this sub-section where the advection, diffusion, and evaporation terms do not vanish.

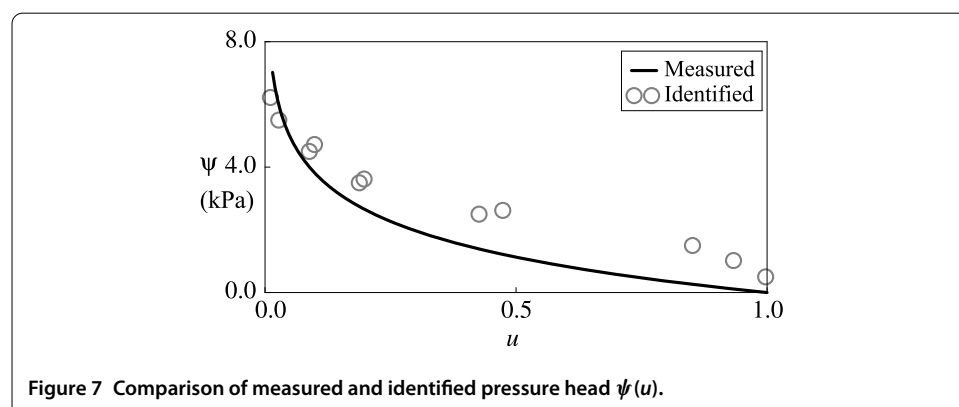
4.2.1 Parameter identification

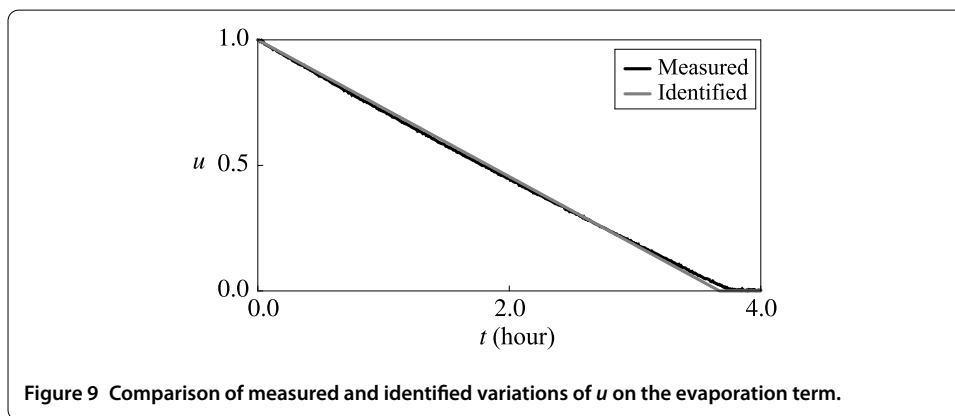
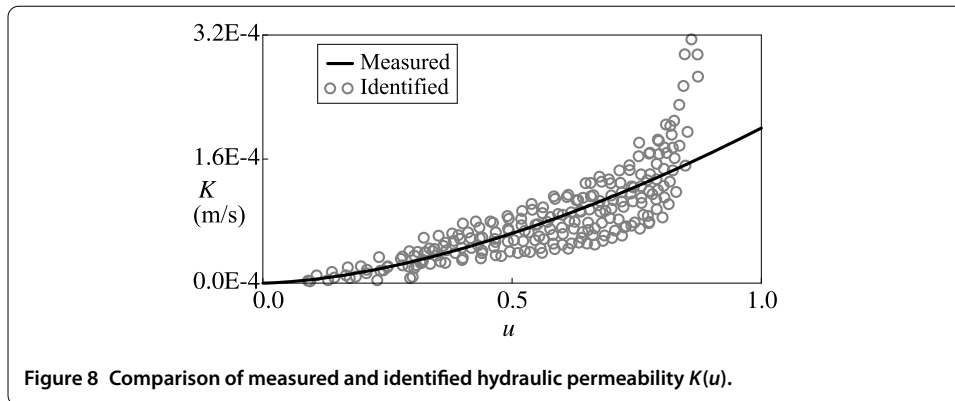
To be used in applications, the extended PME has three coefficients of the functions of u to be estimated: the pressure head $\psi(u)$, the hydraulic permeability $K(u)$, and the evaporation rate $E_s u^q$. This sub-section presents our experimental results to identify reasonable ranges of the parameters involved in these coefficients. In the experiments, a non-woven fibrous sheet for water absorption was used where the product number is not presented in this paper. Thickness of the sheet is 10^{-3} (m). The company manufactured this product for multiple purposes, such as materials for vehicles, materials used in civil engineering, water transportation and adsorption in agricultural fields, and sanitary purposes. The parameters θ_M and θ_r for this sheet has been estimated as $\theta_M = 0.48$ and $\theta_r = 0.07$, respectively.

Pressure head As in the case for the conventional hanging water column method to be applied to soil materials [73], matric potential was steadily controlled for each fixed pressure $-n$ (kPa) with non-negative integers $0 \leq n \leq 6$. The moisture weight percentage of the material, which is denoted by w , was measured at each value of the matric potential. This experiment was repeated twice to reduce statistical errors in the identification process of the matric potential. A standard nonlinear least square method is applied to identify the pressure head $\psi(u)$.

Figure 7 presents the measured and identified $\psi(u)$ where the identified parameter values are $p = 1.5 \times 10^{-2}$ and $\frac{\theta_s D_s}{p K_s} = 1.08 \times 10^2$. The identified $\psi(u)$ underestimates the measured counterpart except for small u , which possibly results in overestimation (underestimation) of capillary transport for small (large) u . It would be possible to find more complex but more accurate parameterization of $\psi(u)$ to improve this problem; however, the PMEs with such a coefficient can have higher nonlinearity that is possibly more difficult to numerically deal with. This topic is approached in future research and is not focused in this paper. The same applies to the other coefficients.

Hydraulic permeability A tensiometer (Stec Co., Ltd.) was utilized. At the beginning of the experiment, a sheet material that is fully wet was prepared, and it was drained from the wet state until it finalizes the drainage of water. During the drainage process, pressure, moisture flux, and moisture weight percentage of the material were measured at one-second interval. This experiment was carried out seven times to reduce statistical errors in the identification process of the hydraulic permeability: four times with the pressure head of -25 (cm) and the remaining three with -35 (cm). The length of the period





for the drainage was 40 to 50 (min). Assuming the conventional Darcy's flux [73], the hydraulic permeability was identified from the experimental results. A standard nonlinear least square method is applied to identify the hydraulic permeability $K(u)$ as a function of u .

Figure 8 presents the measured and identified $K(u)$ with the identified parameter values of $K_s = 2.00 \times 10^{-5}$ (m/s) and $m = 1.64$. The parameter $\frac{\theta_s D_s}{\rho K_s} = 1.08 \times 10^2$ is thus identified as $D_s = 6.75 \times 10^{-5}$ (m^2/s). The measured $K(u)$ for each u is subject to fluctuation because of experimental errors. The identified $K(u)$ is found to be an almost median of the measured counterpart for each u . The identified $K(u)$ thus reasonably reproduces the measured counterpart, and both of them qualitatively and qualitatively agree well.

Evaporation rate The evaporation term is identified with a fully wetted sheet placed in a nearly temporally homogenous environment (a closed laboratory room) where the relative of about 42% to 44% and the temperature of 25 to 26 degree Celsius. The experimental setting is simple: a fully wetted sheet is placed on an electric balance and its weight is measured at the interval of 30 seconds. The measured data is calibrated with analytical solutions to the ODE $\frac{du}{dt} = -E_s u^q$. A standard nonlinear least square method is applied to identify the parameters q and E_s .

Figure 9 presents the measured and identified time series of u . The identified parameter values in the dimensional form are $q = 2.00 \times 10^{-2}$ and $E_s = 8.06 \times 10^{-5}$ (1/s). Figure 10 shows that the present evaporation term can reasonably reproduces the measured varia-

tion of u . Both the measured and identified time series of u agrees reasonably well except for small u despite the present parameterization for the evaporation term is very simple.

4.2.2 Computational examples

An application of the presented mathematical model and the numerical method to moisture dynamics in the non-woven fibrous sheet is carried out where it is placed horizontally ($\alpha = 0$) or vertically ($\alpha = 0.5\pi$). The identified coefficients and parameters in the previous sub-sections are used in the numerical simulation here. The focus here is to track moisture dynamics in a sheet with the two contrasting placement patterns under an evaporative environment.

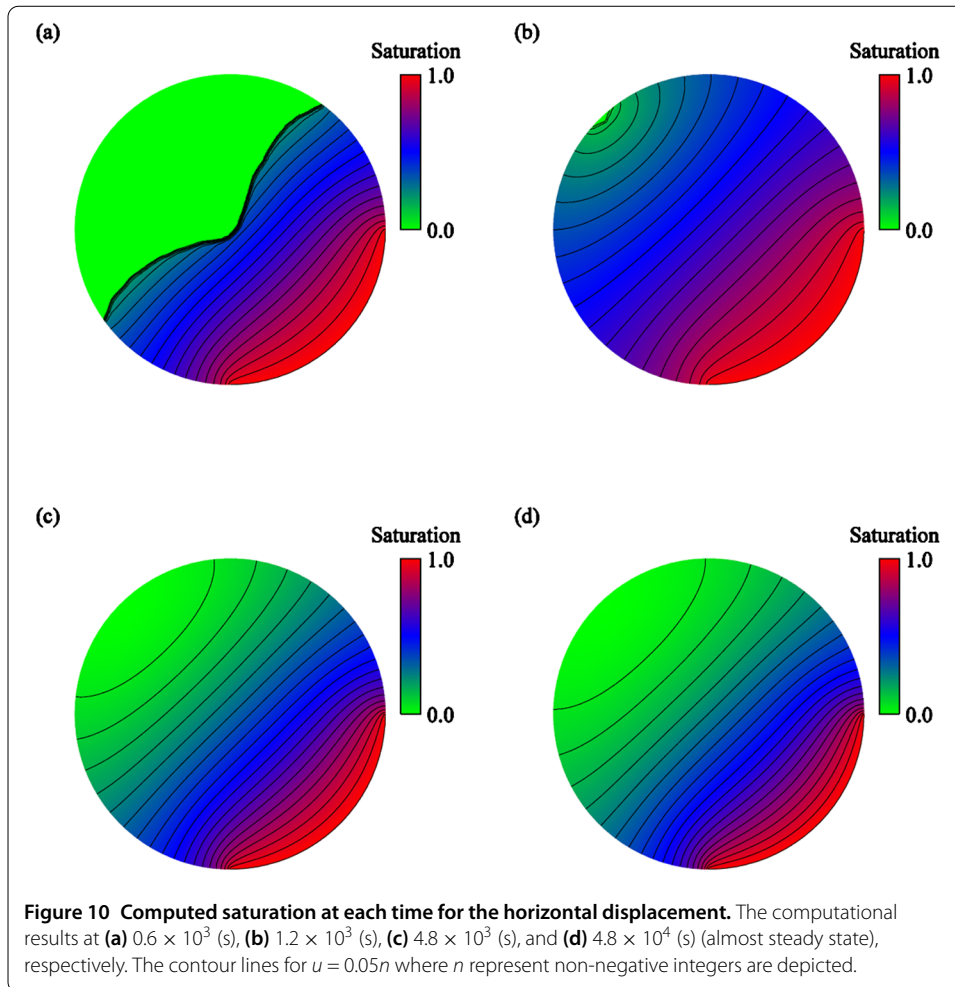
A sheet with a circular shape with the radius of 0.05 (m) is considered, which is considered as the domain $\Omega = \{(x_1, x_2) \mid x_1^2 + x_2^2 < 0.05^2\}$ in the dimensional form. The finest computational mesh for the unit circular domain with 38,588 triangular cells and 19,565 dual cells is used where its spatial scale has been accordingly changed so that the above-mentioned domain is created. The sheet is initially assumed to be dry ($u = 0$), which is specified as the initial condition at the time $t = 0$ (s). The part of the boundary of the domain (x_1, x_2) with $0 \leq x_1 \leq 0.05$ (m) in the dimensional form is assumed to be fully wet ($u = 1$) and the other part of the boundary is considered as the no-flux boundary with the conventional zero-flux condition. The time increment Δt is set as 0.001 in the non-dimensional form, which corresponds to 24.0 (s) in the dimensional form.

Figure 10(a) through 10(d) present the computed saturation at the times 0.6×10^3 (s), 1.2×10^3 (s), 4.8×10^3 (s), and 4.8×10^4 (s) (almost steady state) for the horizontal displacement, respectively. Similarly, Figure 11(a) through 11(d) present the computed saturation at the times 0.6×10^3 (s), 1.2×10^3 (s), 4.8×10^3 (s), and 4.8×10^4 (s) for the vertical displacement, respectively. The spatial distributions of the saturation u at the transient states (Figures 10(a) through 10(c) and 11(a) through 11(c)) are not significantly different between the horizontal and vertical placements; however, they are qualitatively different at the steady state (Figures 10(d) and 11(d)). The spatial distribution of the saturation u at the steady state for the horizontal placement is symmetric with respect to the line $x_1 + x_2 = 0$, but that for the vertical placement is not. This is because the moisture transport is (is not) subject to the gravitational effect for the vertical (horizontal) placement modelled with the nonlinear advection term. Figures 10(a) and 11(a) show that the sharp transitions of the solutions are reasonably captured without numerical failure. The obtained computational results show that the numerical solutions obtained do not have unphysical oscillations, overshoots, and undershoots, indicating that the present 2-D DFVM is able to effectively simulating moisture dynamics subject to the evaporation.

It should be finally noted that both the IS scheme has also been applied to the numerical simulation, but relative error between the numerical solutions with the FU and IS schemes was smaller than several percent. This is considered to be due to the relationship $m \gg p$ for the examined non-woven fibrous sheet where p is sufficiently small to affect the isotonicity of the IS scheme established at $p = 0$.

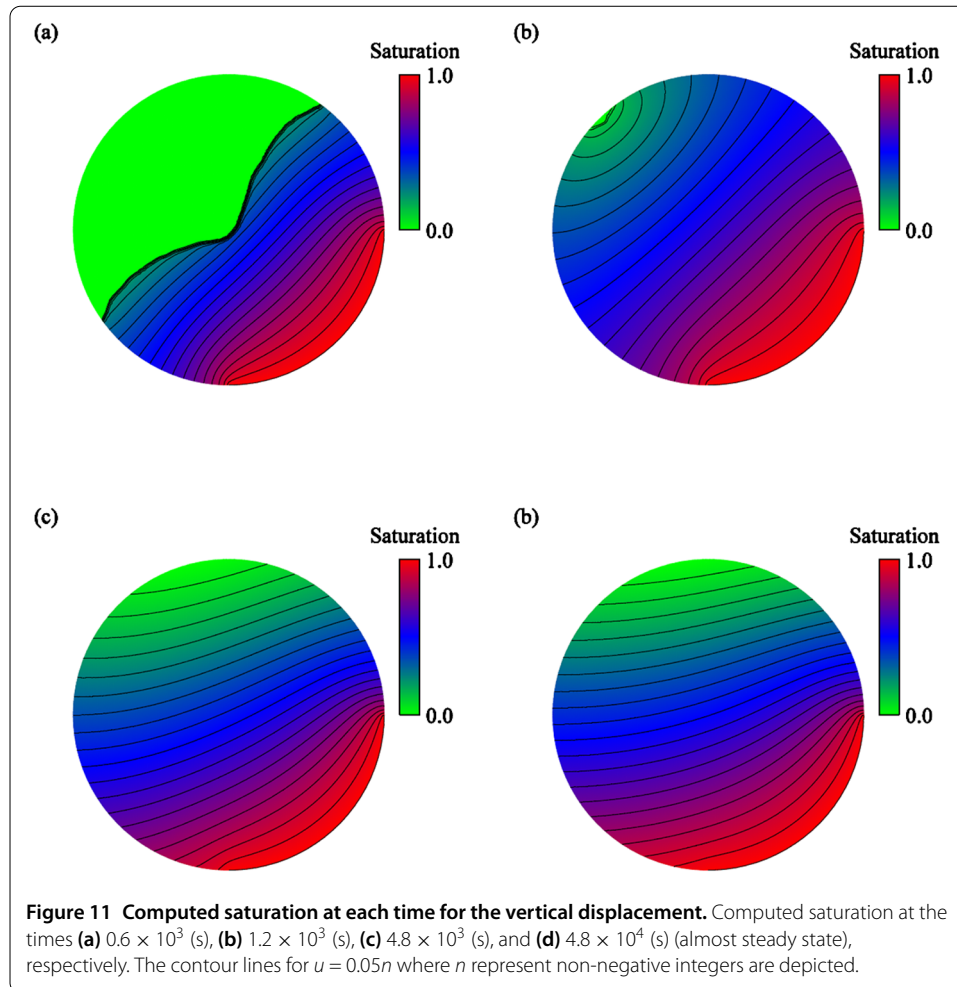
5 Conclusions

This paper presented the 2-D extended PME for moisture dynamics in fibrous sheets under evaporative environment. Each coefficient involved in the 2-D extended PME is possible to identify with physical experiments, and this statement was checked with laboratory experiments. The 2-D DFVM for approximating solutions to the equation was also



presented in this paper with detailed spatial and temporal integration schemes. The concept of isotonicity was effectively incorporated into the evaluation of the numerical flux to compute physically reasonable numerical solutions. An operator-splitting technique based on the analytical solutions to the ODEs was applied to the temporal discretization procedure to handle the problems with nonlinear source terms. Application of the 2-D DFVM to test cases demonstrated its satisfactory computational accuracy and stability. A demonstrative application example of the 2-D extended PME and the DFVM showed their potentially high functionality to simulating essentially 2-D moisture dynamics in fibrous sheets under evaporative environment.

Although this paper focused solely on the moisture dynamics in fibrous sheets, the presented model can be applied to the dynamics in other materials, such as papers, and even to different phenomena if the coefficients involved in the PME are appropriately modified [74–76]. The present DFVM can be used for solving similar differential equations arising in the other research areas where the equations of the PME-type are of central use. Future research will focus on exploring more relevant functional forms of the coefficients of the extended PMEs based on physical experiments, which requires sampling larger number of measured data with higher accuracy. Although the 2-D extended PME assumed homogeneity and isotropy of sheets, real problems of moisture dynamics in non-woven



fibrous sheets would involve spatially heterogeneous and/or anisotropic sheets. Heterogeneity can be partly resolved with the parameters or the coefficients, but appropriate internal boundary conditions will be necessary on the boundary of heterogeneity as in Kuraz et al. [77, 78]. Transport phenomena of chemical substances whose dynamics typically follows certain conservation laws can be simulated based on the moisture dynamics with the present model. From a mathematical side, theoretical numerical analysis of the 2-D DFVM will be performed to deeper comprehend its properties, theoretical order of convergence in particular. Mathematical analysis on the regularization for the nonlinear degenerate parabolic PDEs like PME will also be addressed. Approaching from mathematical, experimental, and numerical sides to these un-resolved issues will be carried out in future research.

Acknowledgements

The authors thank to the reviewers for providing valuable comments on this paper.

Funding

Japan Society for the Promotion of Science, Research Grant No. 17K15345 partly supports the mathematical analysis part of this research.

Competing interests

The authors declare that they have no competing interests.

Authors' contributions

HY wrote the paper and performed mathematical and numerical analysis. KF and IK carried out laboratory experiments.

Authors' information

This paper is a summary of theoretical and experimental analysis carried out by the authors in Shimane University during 2016.

Publisher's Note

Springer Nature remains neutral with regard to jurisdictional claims in published maps and institutional affiliations.

Received: 17 January 2017 Accepted: 14 July 2017 Published online: 28 July 2017

References

- Abidin MSBZ, Shibusawa S, Ohaba M, Li Q, Khalid MB. Capillary flow responses in a soil-plant system for modified subsurface precision irrigation. *Precis Agric.* 2014;15:17-30.
- Bandyopadhyay A, Ramarao BV, Ramaswamy S. Transient moisture diffusion through paperboard materials. *Colloids Surf A, Physicochem Eng Asp.* 2002;206:455-67.
- Bozigian HP, Gendron G, Roberts J. Absorbent hydrogel particles and use thereof in wound dressings. 1999. United States Patent No. 5977428.
- Lockington DA, Parlange JY, Lenkopane M. Capillary absorption in fibrous sheets and surfaces subject to evaporation. *Transp Porous Media.* 2008;68:29-36.
- Ramarao BV. Moisture sorption and transport processes in paper materials. In: Dąbrowski A, editor. *Studies in surface science and catalysis.* Amsterdam: Elsevier; 1999. p. 531-60.
- Yoshioka H, Kita I, Fukada K. Numerical modelling of nonlinear and degenerate diffusion equations on connected graphs: application to moisture dynamics in non-woven fibrous strip networks. *Jpn Soc Industr Appl Math Lett.* 2016;8:45-8.
- Prakotmak P, Soponronnarit S, Prachayawarakorn S. Design of porous banana foam mat to resist moisture migration using a 2-D stochastic pore network and its textural property. *Dry Technol.* 2014;32(8):981-91.
- Zheng J, Shi X, Shi J, Chen Z. Pore structure reconstruction and moisture migration in porous media. *Fractals.* 2014;22(3):1440007.
- Mikhailov MD, Shishedjiev BK. Temperature and moisture distributions during contact drying of a moist porous sheet. *Int J Heat Mass Transf.* 1975;18(1):15-24.
- Cheroto S, Silva Guigon SM, Ribeiro JW, Cotta RM. Lumped-differential formulations for drying in capillary porous media. *Dry Technol.* 1997;15:811-35.
- Kumar D, Kumar V, Singh VP. Modeling and dynamic simulation of mixed feed multi-effect evaporators in paper industry. *Appl Math Model.* 2013;37(1):384-97.
- Polishchuk A, et al. Cultivation of nannochloropsis for eicosapentaenoic acid production in wastewaters of pulp and paper industry. *Bioresour Technol.* 2015;193:469-76.
- Fontana É, et al. Mathematical modeling and numerical simulation of heat and moisture transfer in a porous textile medium. *J Text Inst.* 2016;107(5):672-82.
- Landau LD, Lifshitz EM, Pitaevskii LP. *Electrodynamics of continuous media.* 2nd ed. Oxford: Pergamon Press; 1984.
- Landau LD, Lifshitz EM. *Fluid mechanics.* 2nd ed. Oxford: Pergamon Press; 1959.
- Barth T, Oehlberger M. *Finite volume methods: foundation and analysis.* *Encyclo Comput Mech.* 2004. doi:10.1002/0470091355.ecm010.
- Toro EF. *Riemann solvers and numerical methods for fluid dynamics: a practical introduction.* 3rd ed. Berlin: Springer; 2009.
- Toro EF, Garcia-Navarro P. Godunov-type methods for free-surface shallow water flows: a review. *J Hydraul Res.* 2007;45:736-51.
- Bessemoulin-Chatard M, Filbet F. A finite volume scheme for nonlinear degenerate parabolic equations. *SIAM J Sci Comput.* 2012;34:559-83.
- Kurganov A, Tadmor E. New high-resolution central schemes for nonlinear conservation laws and convection-diffusion equations. *J Comput Phys.* 2000;160:241-82.
- Radu FA, Pop IS, Knabner P. Error estimates for a mixed finite element discretization of some degenerate parabolic equations. *Numer Math.* 2008;109:285-311.
- Fasano A, Primicerio M. Liquid flow in partially saturated porous media. *IMA J Appl Math.* 1979;23:503-17.
- laia J, Betelú S. Solutions of the porous medium equation with degenerate interfaces. *Eur J Appl Math.* 2013;24:315-41.
- Zhang Q, Wu ZL. Numerical simulation for porous medium equation by local discontinuous Galerkin finite element method. *J Sci Comput.* 2009;38:127-48.
- Espedal MS, Karlsen KH. Numerical solution of reservoir flow models based on large time step operator splitting algorithms. In: Fasano A, editor. *Filtration in porous media and industrial application.* Berlin: Springer; 2000. p. 9-77.
- Jakobsen ER, Karlsen KH, Risebro NH. On the convergence rate of operator splitting for Hamilton-Jacobi equations with source terms. *SIAM J Numer Anal.* 2001;39:499-518.
- Hayek M. Analytical solution to transient Richards' equation with realistic water profiles for vertical infiltration and parameter estimation. *Water Resour Res.* 2016;52:4438-57.
- Szymkiewicz A, Helmig R. Comparison of conductivity averaging methods for one-dimensional unsaturated flow in layered soils. *Adv Water Resour.* 2011;34:1012-25.
- Zha Y, Yang J, Shi L, Song X. Simulating one-dimensional unsaturated flow in heterogeneous soils with water content-based Richards equation. *Vadose Zone J.* 2013. doi:10.2136/vzj2012.0109.
- Ashari A, Bucher TM, Vahedi-Tafreshi H, Tahir MA, Rahman MSA. Modeling fluid spread in thin fibrous sheets: effects of fiber orientation. *Int J Heat Mass Transf.* 2010;53:1750-8.

31. Landeryou M, Eames I, Cottenden A. Infiltration into inclined fibrous sheets. *J Fluid Mech.* 2005;529:173-93.
32. Pudasaini SP. A novel description of fluid flow in porous and debris materials. *Eng Geol.* 2016;202:62-73.
33. Bertsch M. Asymptotic behavior of solutions of a nonlinear diffusion equation. *SIAM J Appl Math.* 1982;42:66-76.
34. Wilhelmsson H. Simultaneous diffusion and reaction processes in plasma dynamics. *Phys Rev A.* 1988;38:1482-9.
35. Lakkis I, Ghoniem AF. Axisymmetric vortex method for low-Mach number, diffusion-controlled combustion. *J Comput Phys.* 2003;184:435-75.
36. Rida SZ. Approximate analytical solutions of generalized linear and nonlinear reaction-diffusion equations in an infinite domain. *Phys Lett A.* 2010;374:829-35.
37. Okrasinski W, Parra MI, Cuadros F. Modeling evaporation using a nonlinear diffusion equation. *J Math Chem.* 2001;30:195-202.
38. Borsche R, Gottlich S, Klar A, Schillen P. The scalar Keller-Segel model on networks. *Math Models Methods Appl Sci.* 2014;24:221-47.
39. Tao Y, Winkler M. Global existence and boundedness in a Keller-Segel-Stokes model with arbitrary porous medium diffusion. *Discrete Contin Dyn Syst.* 2012;32:1901-14.
40. Haerens V, van Gorder RA. Classical implicit travelling wave solutions for a quasilinear convection-diffusion equation. *New Astron.* 2012;17:705-10.
41. Antontsev S, Díaz JI, Shmarev S. Energy methods for free boundary problems: applications to non-linear PDEs and fluid mechanics. 1st ed. Boston: Birkhäuser; 2002.
42. Antontsev S, Shmarev S. Evolution PDEs with nonstandard growth conditions: existence, uniqueness, localization, blow-up. 1st ed. Paris: Atlantis Press; 2015.
43. Aronson DG. The focusing problem for the porous medium equation: experiment, simulation and analysis. *Nonlinear Anal, Theory Methods Appl.* 2016;137:135-47.
44. Zambra CE, Dumbser M, Toro EF, Moraga NO. A novel numerical method of high-order accuracy for flow in unsaturated porous media. *Int J Numer Methods Eng.* 2012;89:227-40.
45. Yan J. A new nonsymmetric discontinuous Galerkin method for time dependent convection diffusion equations. *J Sci Comput.* 2013;54:663-83.
46. Albets-Chiko X, Kassians S. A consistent velocity approximation for variable-density flow and transport in porous media. *J Hydrol.* 2013;507:33-51.
47. Cumming B, Moroney T, Yurner I. A mass-conservative control volume-finite element method for solving Richards' equation in heterogeneous porous media. *BIT Numer Math.* 2011;51:845-64.
48. Ortega JM, Rheinboldt WC. Iterative solution of nonlinear equations in several variables. 2nd ed. New York: Academic Press; 1970.
49. Fuhrmann J, Langmach H. Stability and existence of solutions of time-implicit finite volume schemes for viscous nonlinear conservation laws. *Appl Numer Math.* 2001;37:201-30.
50. Yoshioka H, Triadis D. A regularized finite volume numerical method for the extended porous medium equation relevant to moisture dynamics with evaporation in non-woven fibrous sheets. In: Ohn SY, Chi SD, editors. Model design and simulation analysis. Singapore: Springer; 2016. p. 3-16.
51. Yoshioka H, Unami K. A cell-vertex finite volume scheme for solute transport equations in open channel networks. *Probab Eng Mech.* 2013;31:30-8.
52. Chernogorova T, Valkov R. Finite volume difference scheme for a degenerate parabolic equation in the zero-coupon bond pricing. *Math Comput Model.* 2011;54:2659-71.
53. Wang S, Zhang S, Fang Z. A superconvergent fitted finite volume method for Black-Scholes equations governing European and American option valuation. *Numer Methods Partial Differ Equ.* 2014;31:1190-208.
54. Richardson S, Wang S. Numerical solution of Hamilton-Jacobi-Bellman equations by an exponentially fitted finite volume method. *Optimization.* 2006;55:121-40.
55. Fiebach A, Glitzy A, Linke A. Uniform global bounds for solutions of an implicit Voronoi finite volume method for reaction-diffusion problems. *Numer Math.* 2014;128:31-72.
56. Fuhrmann J, Linke A, Langmach H. A numerical method for mass conservative coupling between fluid flow and solute transport. *Appl Numer Math.* 2011;61:530-53.
57. Roos HG. The ways to generate the Π -in and related schemes. *J Comput Appl Math.* 1994;53:43-59.
58. Wang S. A novel fitted finite volume method for the Black-Scholes equation governing option pricing. *IMA J Numer Anal.* 2004;24:699-720.
59. Li Y, Lee G, Jeong D, Kim J. An unconditionally stable hybrid numerical method for solving the Allen-Cahn equation. *Comput Math Appl.* 2010;60:1591-606.
60. Broadbridge P, White I. Constant rate rainfall infiltration: a versatile nonlinear model: 1. Analytic solution *Water Resour Res.* 1988;24:145-54.
61. Masoodi R, Pillai KM. Darcy's law-based model for wicking in paper-like swelling porous media. *AIChE J.* 2010;56:2257-67.
62. Stewart JM, Broadbridge P. Calculation of humidity during evaporation from soil. *Adv Water Resour.* 1999;22:495-505.
63. Yoshioka H, Unami K, Fujihara M. A Petrov-Galerkin finite element scheme for 1-D time-independent Hamilton-Jacobi-Bellman equations. *J Jpn Soc Civil Eng Ser A2.* 2015;71:1_149-1_160.
64. Mishev ID. Finite volume methods on Voronoi meshes. *Numer Methods Partial Differ Equ.* 1998;14:193-212.
65. Lee HG, Lee JY. A second order operator splitting method for Allen-Cahn type equations with nonlinear source terms. *Physica A.* 2015;432:24-34.
66. Lee HG, Shin J, Lee JY. First and second order operator splitting methods for the phase field crystal equation. *J Comput Phys.* 2015;299:82-91.
67. Pop IS, Radu F, Knabner P. Mixed finite elements for the Richards' equation: linearization procedure. *J Comput Appl Math.* 2004;168:365-73.
68. Knabner P, Angermann L. Numerical methods for elliptic and parabolic partial differential equations. 1st ed. New York: Springer; 2003.
69. Barenblatt GI. On self-similar motions of compressible fluid in a porous medium. *Prikl Mat Meh.* 1952;16:679-98.
70. Nasserri M, Daneshbod Y, Pirouz MD, Rakhshandehroo GR, Shirzad A. New analytical solution to water content simulation in porous media. *J Irrig Drain Eng.* 2011;138:328-35.

71. Liu X, Qu C. Long-time behaviour of solutions of a class of nonlinear parabolic equations. *Nonlinear Anal, Theory Methods Appl.* 2008;69:4470-81.
72. Vázquez JL. *The porous medium equation: mathematical theory.* Oxford: Oxford University Press; 2007.
73. Jury W, Horton R. *Soil physics.* 6th ed. Hoboken: Wiley; 2004.
74. Cho CH. On the finite difference approximation for blow-up solutions of the porous medium equation with a source. *Appl Numer Math.* 2013;65:1-26.
75. Dimova M, Dimova S, Vasileva D. Numerical investigation of a new class of waves in an open nonlinear heat-conducting medium. *Cent Eur J Math.* 2013;11:1375-91.
76. Guo L, Yang Y. Positivity preserving high-order local discontinuous Galerkin method for parabolic equations with blow-up solutions. *J Comput Phys.* 2015;289:181-95.
77. Kuraz M, Mayer P, Havlicek V, Pech P. Domain decomposition adaptivity for the Richards equation model. *Computing.* 2013;95:501-19.
78. Kuraz M, Mayer P, Pech P. Solving the nonlinear Richards equation model with adaptive domain decomposition. *J Comput Appl Math.* 2014;270:2-11.

Submit your manuscript to a SpringerOpen[®] journal and benefit from:

- Convenient online submission
- Rigorous peer review
- Open access: articles freely available online
- High visibility within the field
- Retaining the copyright to your article

Submit your next manuscript at ► springeropen.com
